Nanoscale

Accepted Manuscript

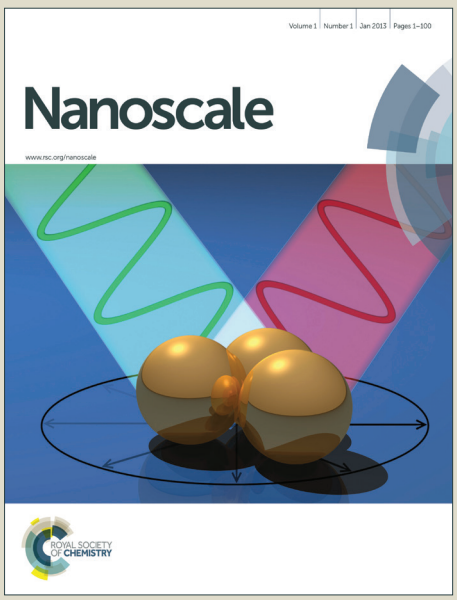

ROYAL SOCIETY OF CHEMISTRY

www.rsc.org/nanoscale

Nanoscale

ARTICLE

Biotransformation of magnetic nanoparticles as a function of the coating in a rat model

Received,
Accepted

DOI: 10.1039/x0xx00000x

www.rsc.org/

A. Ruiz[a,b], L. Gutiérrez[a], P. R. Cáceres-Vélez[c], D. Santos[c], S. B. Chaves[c], M. L. Fascineli[c], M. P. Garcia[c], R. B. Azevedo[c], M. P. Morales[a]*

Long-term *in vivo* studies in murine models have shown that DMSA-coated nanoparticles accumulate in spleen, liver and lungs tissues during extended periods of time (at least up to 3 months) without any significant signs of toxicity detected. During that time, nanoparticles undergo a process of biotransformation either reducing the size, the particle aggregation or both. Using a rat model, we have evaluated the transformations of magnetic nanoparticles injected at low doses. Two particles with different coatings, dimercaptosuccinic acid (NP-DMSA) and polyethylene glycol (NP-PEG-$(NH_2)_2$ have been administered to the animals, to evaluate the role of the coating in the degradation of the particles. We have found that low doses of magnetic nanoparticles are quickly metabolized by the animals. In fact, using a nanoparticle dose four times lower than in previous experiments, NP-DMSA were not observed 24 h after the administration either in the liver or the lungs. Interestingly, an increased amount of ferritin, the iron storage protein, was observed in liver tissues from rats that were treated with the low dose of NP-DMSA in comparison with the control ones, suggesting a rapid metabolization of the particles into ferritin iron. On the other side we have found that, NP-PEG-$(NH_2)_2$ are still detectable in several organs 24 h after their administration at low doses. Probably, due to the longer circulation times of the NP-PEG-$(NH_2)_2$, there is a delay on the arrival of the particles to the tissue and this is the reason why we are able to see the particles 24 h post-administration. PEG coating could also be protecting the nanoparticles from rapid degradation of the reticuloendothelial system. Knowledge on the biodistribution, circulation time and degradation processes is required to gain a better understanding on the safety evaluation of this kind of nanomaterials for biomedical applications.

Keywords: Iron oxide nanoparticles, PEG, AC susceptibility, biodistribution, biotransformation, metabolism

Introduction

Iron oxide magnetic nanoparticles are presently being employed in a wide variety of biomedical and biological applications such as contrast enhancement of magnetic resonance imaging (MRI), targeted drug or gene delivery, tissue engineering, hyperthermia in cancer therapy, cell labelling, cell sorting and immunoassay[1-3]. It is currently the most popular superparamagnetic material used *in vivo*, with several commercialized products used as contrast agents or at different stages of clinical trials[4].

Nanoparticles (NP) safety and effective performance *in vivo* are influenced by their biodistribution and clearance in the body. The latter is determined by nanoparticle physicochemical properties such as size, charge, decoration by functional groups or functionalization with biomolecules. Consequently, many research efforts are presently focused on the life cycle and toxicity of these nanomaterials. However it is difficult to draw general conclusions about their nanotoxicity due to the material diversity. Even comparing nanotoxicological data of only one type of iron oxide nanoparticle coated with the same anionic molecule, for example, dimercaptosuccinic acid, we found many apparently different results in *in vitro* tests[5]. These contradictory results have been reported due to different cell lines tested, variability in concentrations used, and physical, chemical, and structural properties of magnetic nanoparticles[6].

In recent years different articles showed *in vivo* assessment of DMSA and PEG coated nanoparticles[7-9]. But to ensure biosafety it is important to consider not only pharmacokinetic parameters, biodistribution or immunogenicity, it is also essential to understand the

[a] Instituto de Ciencia de Materiales de Madrid (ICMM)/CSIC, Sor Juana Inés de la Cruz 3, Cantoblanco, 28049 Madrid, Spain. puerto@icmm.csic.es.
[b] 2Centro de Estudios Avanzados de Cuba (CITMA), Carretera San Antonio de los Baños, km $3^{1/2}$ La Lisa, La Habana, Cuba.
[c] Universidad de Brasilia, Campus Universitário Darcy Ribeiro, Brasília - DF, 70910-900, Brasil.

biotransformation of the nanoparticles in different animal models in order to unravel the mechanisms determining their fate. The life cycle of the nanoparticles and their biodegradation products provides relevant information on the design of safer and more efficient nanomaterials[10]. In some applications, such as targeted drug delivery, researchers aim to develop nanoparticles such that they are selectively incorporated by specific cell type[11]. In other applications, such as NP-based contrast agents for magnetic resonance imaging, nanoparticles should stay in the bloodstream for longer periods. Therefore there is a crucial need in controlling the biodegradation of such structures by following their physical properties and morphological transformations.

The pharmacokinetic and biodistribution of DMSA-coated nanoparticles have been described in different animal models such as mice, rats, rabbits and monkeys[12-14]. In general, nanoparticles were detected in liver, lungs and spleen after intravenous injection in mice, although the percentage of particles that goes to this last organ is usually much lower than the other two[12, 15]. These nanoparticles modified with PEG showed doubled residence time than NP-DMSA in blood[13]. The uptake of the nanoparticles by the macrophages of the reticuloendothelial system (RES) has been reported[16] followed by their accumulation in the cytoplasm in acidic compartments (endosomes) for degradation[17]. The biotransformation of the nanoparticles takes place in the lysosomal environment, resulting in a transfer of iron from synthetic particles to ferritin proteins[18]. The combined use of aberration-corrected high resolution transmission electron microscopy and magnetic measurements evidenced the molecular mechanism of iron transfer. *In vitro* experiments suggest a model for nanoparticle degradation, with a reservoir of intact nanoparticles coexisting with rapidly degraded nanocrystals[19]. However, *in vivo* experiments are necessary to identify different iron species and understand the role of iron metabolic proteins involved in the biotransformation of the nanoparticles.

In previous studies, we developed an approach for the synthesis of magnetic nanoparticles coated with DMSA and modified with polyethylene glycol (PEG)-derived molecules[13]. Magnetite nanoparticles were obtained *via* thermal decomposition of an iron coordination complex as a precursor to ensure nanoparticle homogeneity in size and shape. In this work, we have evaluated the transformations of magnetic nanoparticles injected at low doses (2.5 mg Fe/kg B.W.) using a rat model. We have previously studied that it is possible to conduct MRI scanning within 12 days after nanoparticle administration using this doses, which is important for clinical diagnosis[8]. Now we are investigating how the coating of the nanoparticles (one short and highly charged small molecule such as dimercaptosuccinic acid (DMSA), and the other hydrophilic and uncharged like a 2000 Da diamine-PEG polymer) controls the chemical-physical evolution of the nanoparticles after intravenous injection and the iron transfer and recycling into ferritin storage proteins.

Nanoparticle detection, accumulation and degradation were followed by histopathological studies and magnetic measurements, in particular AC susceptibility. This last technique has been showed to be an excellent method to describe *in vitro* the interactions cell-nanoparticles in this complex matrix[20]. The technique also allows to quantify magnetic nanoparticles in tissues, being able to provide information on the particle transformations over time and the distinction of the particles from other endogenous species such as the ferritin iron cores[7].

Experimental

Materials

Iron (III) acetylacetonate, 1,2-dodecanediol, oleic acid, oleylamine, 1-octadecene, hexane, dimercaptosuccinic acid, ethanol, toluene, 1-ethyl-3-(3-dimethylaminopropyl)-carbodiimide hydrochloride and O,O-bis(2-aminoethyl)-polyethylene glycol 2000 Da were commercial products purchased from Sigma-Aldrich. Antibodies were purchased in Abcam (Anti-Ferritin antibody (ab75973) and Anti-DMT1 antibody (ab55735) and Anti-Ferroportin antibody (ab85370)). Wistar rats were from the University of Brasilia (Brasilia, Brazil).

Magnetic nanoparticle synthesis and characterization

Magnetite nanoparticles were obtained *via* thermal decomposition of an iron coordination complex as a precursor to ensure nanoparticle homogeneity in size and shape following a method previously reported[13]. Particle size and shape were studied using a 200 keV JEOL-2000 FXII microscope. A drop of a dilute magnetic nanoparticle suspension in hexane was placed on a carbon coated copper grid and dried at 50 ºC. Size distribution was determined through manual measurement of more than 300 particles and data were analyzed with Gwyddion 3.25 software to

obtain the mean size and standard deviation by log-normal fitting. Particles were coated with meso-2,3-dimercaptosuccinic acid (NP-DMSA) by a ligand exchange process to remove oleic acid, after which a short-chain diamine PEG (2000 Da) was covalently bound to the nanoparticle surface *via* 1-ethyl-3-(3-dimethylaminopropyl)-carbodiimide hydrochloride (EDC) activation of the carboxylic acids (NP-PEG-$(NH_2)_2$). Colloidal properties of 0.5 mM Fe nanoparticle suspensions in water were characterized by dynamic light scattering (DLS) using a Nanosizer ZS (Malvern). Z-Average values in intensity at pH 7 were used as the mean hydrodynamic size (D_h). The polydispersity degree index (PDI) was calculated by dividing the standard deviation by the mean size. The ζ-potential was measured in a 0.01 M KNO_3 solution and HNO_3 and KOH to change the pH of the suspensions. Thermogravimetric analysis (TGA) of the magnetic nanoparticle powders was carried out in a Seiko TG/ATD 320 U, SSC 5200. The analysis was performed from room temperature to 1000 ºC at 10 ºC/min with an air flow rate of 100 mL/min. Magnetic measurements were made using a vibrating sample magnetometer (MLVSM9 MagLab 9T, Oxford Instruments). Liquid samples (100 µL) were dried in a piece of cotton and tissue samples were frozen and freeze-dried overnight in a LyoQuest freeze dryer (Telstar). The resulting solid samples were compacted into gelatin capsules for magnetic characterization. Magnetization curves were recorded by saturating the sample in a 1 T field and sweeping the field range between 1 and -1 T at 0.3 T/min. The magnetic characterization was also analyzed in a Quantum Design MPMS-XL SQUID magnetometer with an AC susceptibility option. The measurements were performed with AC amplitude of 0.41 Oe, in the temperature range between 1.8 and 300 K and at a frequency of 11 Hz.

Biodistribution studies

Male Wistar rats (11-12 weeks) weighing 300 ± 20 g (n=4/group per time point) were maintained under controlled conditions before and during the experiments (*i.e.*, room temperature at 25 ºC; relative humidity of 65%; 12 h light/dark cycle). Access to food and water was provided *ad libitum*. All animal procedures were carried out under the approval of the Animal Care and Use Committee of the University of Brasilia.

We studied the biodistribution of NP-DMSA and NP-PEG-$(NH_2)_2$ after nanoparticle injection into the tail vein at a dose of 2.5 mg Fe/kg B.W. (0.5 mL) and progressively animals were sacrificed at 24 hours, 7, 15 and 30 days post injection for the analyses. The liver, lungs, spleen and kidneys were collected and divided in four parts for different test.

Histological evaluation

After extraction one fraction of the organs was fixed in Davidson solution and embedded in paraplast blocks. Sections were deparaffinized and rehydrated before staining. Perls stain was used specifically for iron identification in the tissue. Perls staining was performed using equal volumes of 1 N HCl and 10% potassium ferrocyanide (30 min) and counterstained with 1% neutral red (2 min).

Nanoparticle content analysis

The second and third fractions of the organs were lyophilized overnight in a LyoQuest freeze dryer (Telstar), weighed, and measured the iron content by Inductively Coupled Plasma – Optical Emission Spectrometry (ICP-OES) in a OPTIME 2100DV from Perkin Elmer, after acid digestion or powdered with an agate mortar for magnetic characterization respectively. The sample manipulation was performed using a disposable plastic material to avoid ferromagnetic contamination.

Protein Content

The fourth fraction was stored at -80 °C until analysis. In order to evaluate total proteins by Lowry method[21], fragments of the organs were homogenized at 4 ºC in a buffer solution of sucrose 300 mM, EDTA 100 mM, Triton X-100 0.3%, KH_2PO_4 20 mM, Tris 20 mM, pH 7.4. Protein content was measured and the concentration was adjusted at 1 mg/mL.

Ferritin iron quantification

Quantitative analysis of the ferritin formation has been performed using the previously proposed guidelines[22] allowing the quantification, in tissue samples, of iron in the form of ferritin cores. Ac magnetic susceptibility data from a commercial rat liver ferritin (Sigma) has been used as a standard for ferritin quantification[23].

Enzyme-Linked Immunosorbent Assay

In order to evaluate three key-proteins involved in iron metabolic pathway different ELISAs were performed using the corresponding monoclonal antibodies. Different microtiter plates were prepared for independent analysis of the proteins. Each well was coated with 80 µL of the antibody solution at the corresponding dilution in PBS (Anti-

Ferritin antibody 1: 1000; Anti-DMT1 antibody 3: 1000, Anti-Ferroportin antibody 1: 1000) and incubated over night at 4 ºC. The coated plate was washed twice with 200 µL of PBS and incubated 1 h in assay buffer [PBS solution containing BSA 0.5% (w/v)] (180 µL) at room temperature. Then, 100 µL-diluted samples (1 mg/mL) were added per well in assay buffer. After incubation for 1 h at room temperature, the plate was washed five times with bicarbonate buffer pH 9.6. Then, 70 µL of the corresponding conjugated second antibody, labeled with horseradish peroxidase and diluted 1: 10000 (v/v) in the assay buffer, were added and incubated at room temperature for 1 h. The plate was washed five times with bicarbonate buffer, and then incubated for 30 min with 100 µL of the substrate solution (PNPP 1 mg/mL diluted in diethanolamine 10%, 0.5 mM $MgCl_2$ pH 9.8). Absorbance at 405 nm was measured by using an ELISA-plate reader SpectraMax M2.

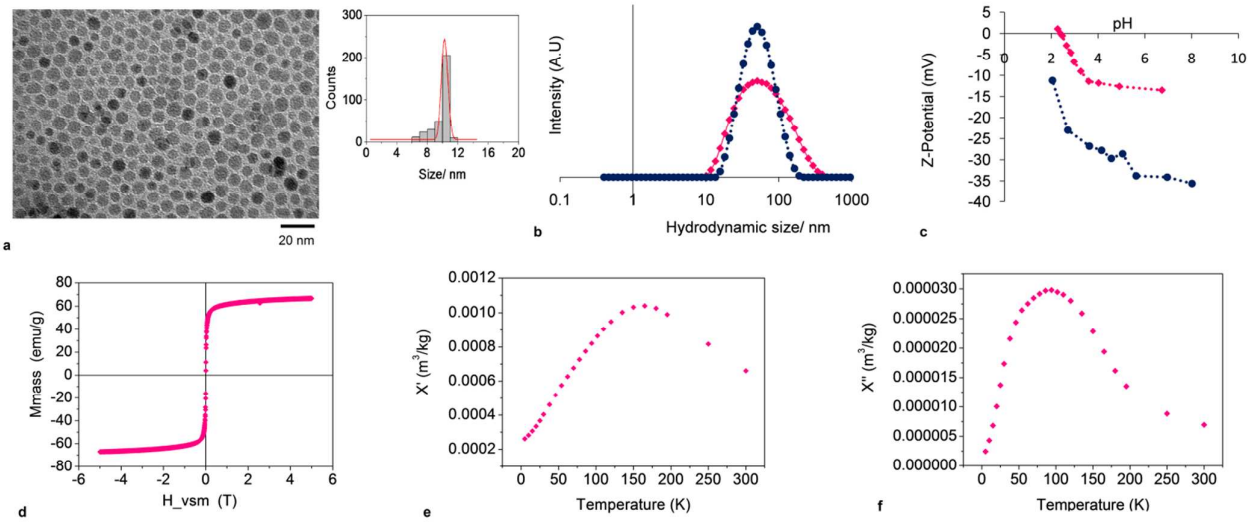

Figure1. (a) Transmission electron microscopy (TEM) images of 10 nm nanoparticles (Scale bar: 20 nm). Size distribution histogram: Red line indicate the log-normal fitting function of TEM particle size data (b) Hydrodynamic sizes for NP-DMSA and NP-PEG-$(NH_2)_2$. (c) Evolution of ζ-potential as a function of pH. (d) Magnetization curve at 250 K for PEG coated nanoparticles. Temperature dependence of the (e) in-phase and (f) out-of-phase components of the susceptibility, per mass of sample, of lyophilized NP-PEG-$(NH_2)_2$. [NP-DMSA ●, NP-PEG-$(NH_2)_2$ ♦]

Results and discussion

Magnetic nanoparticle synthesis and characterization

Iron oxide nanoparticles were synthesized by thermal decomposition of iron (III) acetylacetonate in 1-octadecene. Particles were 10 nm in diameter and showed a very narrow size distribution (PDI = standard deviation/mean size = 0.15). A transmission electron microscopy (TEM) image of this sample is shown in Figure 1a. To obtain a stable colloidal dispersion in water our approach is based on a ligand exchange reaction with DMSA (NP-DMSA). This replaces the oleic acid coating agent with DMSA, resulting in nanoparticles with good water stability and a functional group that can be potentially used for further conjugation with diamine-PEG derivative *via* EDC-mediated coupling reaction (NP-PEG-$(NH_2)_2$). Dispersions in water of NP-DMSA present long-term stability at room temperature (20-25 ºC) or in the refrigerator (4 ºC). Thus, after being stored at 4 ºC for more than 10 months, no changes in the hydrodynamic size (as checked by DLS), the magnetic properties (as checked by VSM) or sedimentation were observed[24]. The hydrodynamic size of the particles, was measured with dynamic light scattering. Hydrodynamic sizes of 42 nm (PDI 0.161) and 50 nm (PDI 0.215) were obtained for NP-DMSA and NP-PEG-$(NH_2)_2$, respectively, and polydispersity degrees (PDI) were lower than 0.25 showing a monomodal distribution (Figure 1b). PEG modification increases surface charge from approximately -35 mV for NP-DMSA samples to -15 mV for PEG-conjugated samples at physiological pH (Figure 1c). Thermogravimetric (TG) analysis of the unconjugated nanoparticles (NP-DMSA) reveals a weight loss of ~13 %, due to the removal of physical and chemically adsorbed water and DMSA molecules. Samples conjugated

to PEG-$(NH_2)_2$ had a total weight loss of 28 %. Taking into account the nanoparticle surface area and the amount of PEG, the presence of ~3 molecules/nm^2 was determined for diamine-PEG in the thermogravimetric analysis. Surface density of the polymer suggests an extended conformation of the PEG molecules at the nanoparticle surface. These results are in agreement with previous observations of particle stability in presence of surfactants[13]. These analyses clearly showed that the PEG coating influences the physical properties of the particles. This is closely linked with lower uptake of nanoparticles in macrophage cells, reduced particle interactions with plasma proteins involved in immune activation, opsonization and attachment of the nanoparticles to the cell membrane and increased circulatory half life. The uncharged nature of this polymer, render these PEG-coated nanoparticles ''invisible'' to the inmune system, making them attractive for biomasking strategies[25].

Magnetization curves were performed to study the magnetic properties of the nanoparticles (Figure 1d). The samples showed superparamagnetic behaviour at 250 K and M_S values measured were around 67 emu/g of nanoparticles. The temperature dependence of the in-phase and out-of-phase components of the susceptibility is shown in Figures 1e and 1f. The out-of-phase susceptibility per mass of sample of the magnetic nanoparticles is of key interest, as it will be used as a fingerprint for the identification of the same particles in tissues[12].

Biodistribution

The use of magnetic nanoparticles in nanomedicine and biology implies a necessary understanding about its biodistribution, biotransformation and toxicity. In our studies, the treatment with NPs did not affect the daily animal body weight. No other signs of toxicity were observed during the experiment (seizures, disheveled hair, irregular respiration, gastrointestinal symptoms, immobility, convulsions, severe decubitus paralysis or death). We also monitored the hematological parameters and performed a genotoxicity test to demonstrate the safety of these nanoparticles at the analyzed dose. No significant changes were observed in the cell count, nor hemolysis for NP-DMSA or NP-PEG-$(NH_2)_2$. *In vitro* analyses revealed prolonged aPTT values for NP-DMSA compared with NP-PEG-$(NH_2)_2$, which indicate higher anticoagulant effect for the former, probably due to a higher negative surface charge. The *in vivo* tests showed that these bioferrofluids do not cause genotoxic effects and do not affect erythropoiesis or increase the number of immature erythrocytes in the bone marrow (unpublished results).

We examined the distribution patterns of these nanoparticles in the principal organs involved in the elimination process. Perls staining, specific for iron identification in the tissue, was positive in the liver up to 30 days after nanoparticle injection. Stained areas can be observed as aggregates in the tissue (Figure 2b) or interior of hepatocytes (Figure 2c), especially those around the centrilobular veins. Also, iron aggregates were observed in other areas of the hepatic parenchyma such as the interlobular connective tissue or liver sinusoids. Lungs sections were positive up to 30 days in the case of animals treated with PEG coated nanoparticles, but no stained sections were detected after 24 h of the NP-DMSA injection (Figure 2 e,f). Spleen sections showed stained areas in the red pulp, even in control tissues, possibly due to the storage of iron degradation products as a result of erythrocyte phagocytosis and the presence of metallophilic macrophages[26]. Kidney sections were only positive for Perls staining after 15 days of the administration and this could be explained because superparamagnetic material is biotransformed to other iron forms and can thus be detected in the histological analysis. Presence of NP-DMSA after intravenous injection was also observed in kidney sections and urine pool in monkeys[14]. However, this reaction is non-specific in identifying the different ways in which iron can be found in the organs: bound to ferritin, haemosiderin or forming aggregates of nanoparticles[27]. Apart from this iron accumulation, we found no structural changes or no apparent histopathological abnormalities in comparison with the control in any of the tissues. In order to obtain information on the iron speciation in tissues where Perls staining was positive, a method such as the AC susceptibility that allows the identification and quantification of the iron oxide nanoparticles present in tissues was used[22].

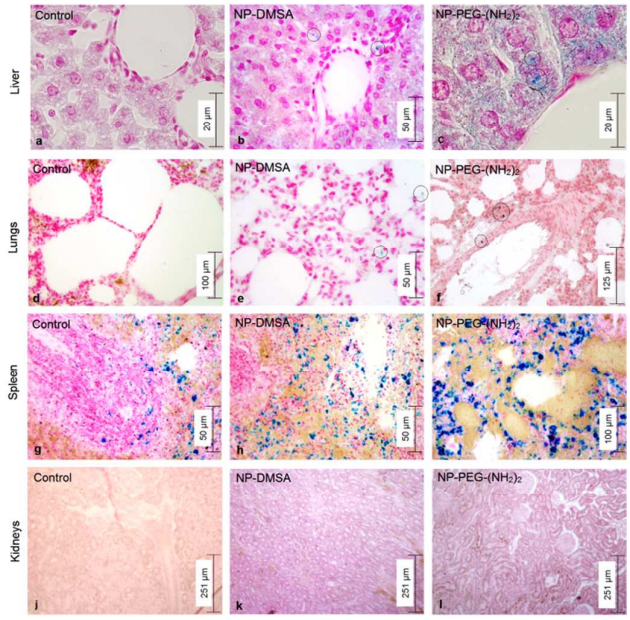

Figure 2. Perls staining of different sections of the organs from rats treated with NPs after 30 days of the injection. (a) Liver Control 30 days. (b) Liver NP-DMSA 24 h. (c) Liver NP-PEG-$(NH_2)_2$ 24 h. (d) Lungs Control 24 h. (e) Lungs NP-DMSA 24 h. (f) Lungs NP-PEG-$(NH_2)_2$ 30 days. (g) Spleen Control 7 days. (h) Spleen NP-DMSA 15 days. (i) Spleen NP-PEG-$(NH_2)_2$ 15 days. (j) Kidneys Control 24 h. (k) Kidneys NP-DMSA 24 h. (l) Kidneys NP-PEG-$(NH_2)_2$ 24 h. Black circles indicates possible aggregates of nanoparticles.

AC magnetic susceptibility

Results from the tissue characterization by AC magnetic susceptibility are shown in Figure 3. The temperature dependence of the out-of-phase susceptibility of the spleen, liver and lungs of control animals together with those corresponding to rats that received a single dose of PEG and DMSA coated nanoparticles and were sacrificed 24 h after the administration are shown in Figures 3 (a – c). Two different contributions to the out-of-phase susceptibility are found in these organs. The maximum located at around 10 K corresponds to the presence of ferritin[23] and the maximum located at higher temperatures (40-50K) corresponds to the administered nanoparticles.

In the control spleen tissues, the presence of iron in the form of ferritin is observed, in agreement with the histological observations that showed Prussian blue stained areas in the control tissues (Figure 2 (g)). Similar amounts of ferritin iron are observed in the treated rats, both with DMSA and PEG coated particles. Interestingly, while no sign of the particles is observed in the NP-DMSA treated animal, the NP-PEG-$(NH_2)_2$ treated animal shows a maximum around 50 K corresponding to the presence of nanoparticles. The difference between the two treatments could be the result of a different biodistribution of the particles, or the quicker degradation of the DMSA-coated particles in comparison with the PEG-coated ones. In the liver tissues, no sign of ferritin iron is observed in the control animal. In comparison, a clear maximum associated to the presence of ferritin is observed in the NP-DMSA treated animal. The animal that was treated with NP-PEG-$(NH_2)_2$, shows both the presence of the particles (with a maximum around 40 K) and ferritin (with a shoulder around 10 K). In the lung tissues, only a weak signal from the particles was observed in the NP-PEG-$(NH_2)_2$ treated animal, while no signs of either the particles or ferritin were observed for the other two animals.

In addition to the study of the presence of either ferritin or the nanoparticles 24 h after their administration, selected tissues from animals sacrificed at longer times after the administration were analyzed. The evolution of the contributions to the out-of-phase susceptibility with time for liver tissues is shown in Figure 3 (d, e). The liver tissues from NP-DMSA treated animals show a high amount of ferritin iron 24 h after the administration that subsequently decreases at 30 days after the administration. The amount of ferritin iron 30 days after the administration is still higher than the control animals. The liver tissues from NP-PEG-$(NH_2)_2$ treated animals show that the magnetic nanoparticles could only be observed 24 h after the administration. In the next time point, at 7 days, only ferritin is observed. Furthermore, the amount of ferritin is reduced at longer times after the administration (30 days). These results demonstrate the quick degradation of the particles and the subsequent generation of ferritin, that is then reduced with time almost reaching control levels. A similar pattern of the quick degradation of the NP-PEG-$(NH_2)_2$ is observed in both the spleen and the lungs (Figure 3 f, g), where the particles are only observed 24 h after the administration.

The amount of ferritin in the liver tissues has been quantified using as a standard a commercial rat liver ferritin. The iron concentration in the form of ferritin determined for livers from the NP-DMSA treated animals is 1 mg Fe/g dry tissue 24 h post-administration, decreasing to 0.7 mg Fe/g dry tissue 30 days post-administration. The livers from NP-PEG-$(NH_2)_2$ treated animals contain 1 mg Fe/g dry tissue 7 days post-administration, decreasing to 0.4 mg Fe/g dry tissue 30 days

post-administration. In this series, it has been impossible to determine with enough accuracy the amount of ferritin iron 24 h post-administration due to the presence of the NP-PEG-$(NH_2)_2$ maximum.

It is interesting to mention that the NP-DMSA have not been observed in any studied tissue, even at the shorter time points (24 h post-administration). Probably, due to the longer circulation times of the NP-PEG-$(NH_2)_2$, there is a delay on the arrival of the particles to the tissue and this is the reason why we are able to see the particles 24 h post-administration only when they are coated with PEG. PEG coating could also be protecting the nanoparticles from rapid degradation inside the cells of the reticuloendothelial system.

It is also worth comparing these results with previous observations on long-term analysis of the biodistribution and degradation processes of magnetic nanoparticles in a murine model[7]. Although the particles used were very similar to the ones analyzed here and the animal models are closely related species, the doses were significantly higher in the murine experiments what justify the presence of particles in tissues 3 months post-administration. This means that there is a dose-response relationship in metabolism although we cannot discard an effect of using different animal models.

It is surprising that no NP-DMSA have been detected in the lung tissues in our experiment, provided that previous studies have shown a preferential targeting of DMSA coated particles to lung tissues in murine models[28-30]. Again, further studies are required to determine if species differences on nanoparticle biodistribution are only related to differences in the metabolism or show a dose-response relationship. A careful inspection of the out-of-phase susceptibility maxima associated to the presence of ferritin reveals a different temperature location of the maxima depending on the organ. Liver tissues present an out-of-phase susceptibility maximum at around 12 K, while the spleen counterparts show a maximum below 10 K. This variance points to a different mineralization process of the iron-containing core in liver and spleen, as observed in an Hfe-haemochromatosis murine model[31]. In normal conditions, ferritin stores iron in the form of ferrihydrite[32], within a shell assembled from 24 subunits of two types, the H subunit (21 kDa) and the L subunit (19 kDa). One possible explanation of the different iron core would be a different iron loading of the ferritin cores, as the observed in *Drosophila Melanogaster* models with either reduced levels of ferritin expression or ferritin overexpression[33]. Another possible explanation is associated to the different H and L subunit ratios of ferritin in these two organs[34].

Nanoscale

ARTICLE

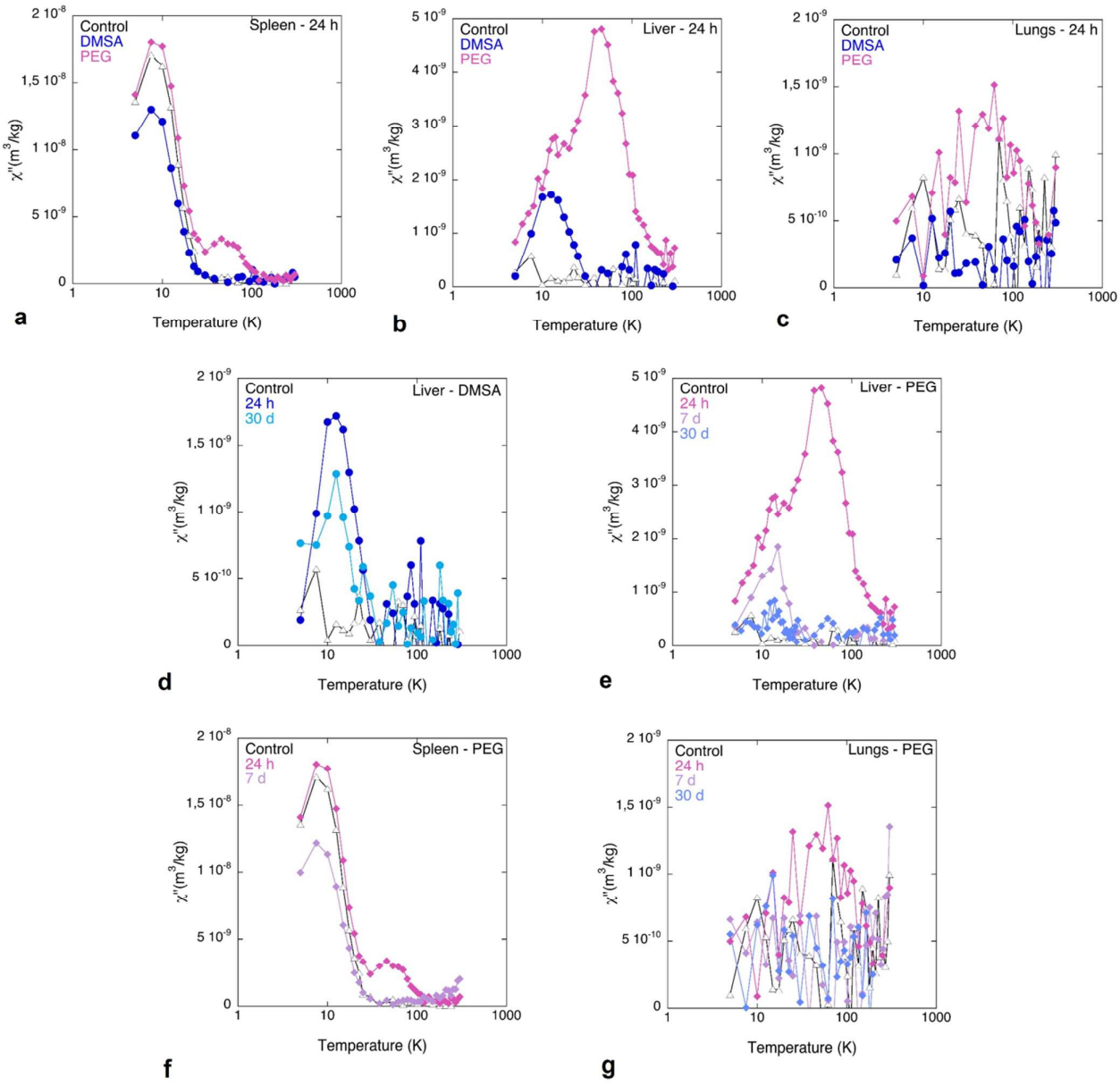

Figure 3. Tissue characterization by AC magnetic susceptibility. Temperature dependence of the out-of-phase component of the magnetic susceptibility, per mass of sample, corresponding to freeze-dried tissues from different organs: (a) Spleen, (b) Liver, (c) Lungs, 24 hours after nanoparticle injection. Evolution of the contributions to the out-of-phase susceptibility with time for DMSA or PEG coated nanoparticles treatments: (d, e) Liver, (f) Spleen and (g) Lungs. [White triangles: control, Blue circles: NP-DMSA, Pink diamonds: NP-PEG-$(NH_2)_2$].

Nanoscale

ARTICLE

The differences observed on the temperature location of the out-of-phase susceptibility maxima between the initial particles, at around 90 K (Figure 1), and the tissue samples, between 40 and 50 K (Figure 3), could be explained by two parameters: the interparticle interactions and the particle size reduction due to their degradation. Agar dilutions of similar particles prepared in order to reduce the interparticle interactions have shown a shift on the temperature location of the out-of-phase susceptibility maximum from 65 K for the more concentrated particles to 35 K for the more diluted ones, with negligible interparticle interactions[12]. A similar shift of the maxima location towards lower temperatures has been observed during long-term experiments following the transformations of DMSA-coated nanoparticles in a murine model. In this case, the out-of phase susceptibility maximum varied from 60 K at the initial times to around 35 K after three months of the administration[7]. Using slightly different particles, Chamorro et al., have also seen transformations on the out-of-phase susceptibility maximum towards lower temperatures during the oral administration of magnetic nanoparticles to growing chickens in their excretion within feces[35].

Iron metabolism

Although there are some previous studies of *in vivo* iron oxide nanoparticles distribution and clearance, little is known of the route of nanoparticle metabolism. With the aim to study the influence of the administration of these nanoparticles in iron metabolism pathways, three key metabolic proteins were selected: DMT1, Ferroportin and Ferritin. DMT1 is a divalent metal transporter 1 (DMT1), involved in the release of iron from the lysosomes into the cytosol. In the cytosol, the iron may be incorporated into the cell metabolism, as the synthesis of heme in mitochondria, or stored as ferritin as it has been recently observed by TEM[36]. Iron can also be exported out of the cell by a transmembrane transporter (ferroportin). Outside the cell, iron is oxidized and transported in the blood, complexed with transferrin, into those organs where the cells have the transferrin receptor in the extracellular membrane: hepatocytes in the liver, erythroblasts in the bone marrow, and red blood cells[37]. Figure 4 shows the variation in time of the concentration of these proteins with respect to baseline levels obtained in the control group. In general, we observed an increase in the concentration of these proteins in the analyzed organs 24 hours after the injection. One day post-injection, ferritin levels increased specially in liver and spleen. Higher levels of ferritin 24 h after injection were observed in animals treated with NP-DMSA. These results confirm the quick biotransformation process of the nanoparticles previously detected by magnetic measurements. More interestingly, ferritin levels remained elevated in kidneys throughout the studied period. These findings support the information obtained by histological analysis in the identification of different iron forms in the kidneys 15 days after the treatment.

DMT1 and ferroportin showed a significant increase in the liver 24 hours after injection. Based on our data we can say that the principal metabolic activity associated with the treatment with iron nanoparticles takes place in the liver. Other organs such as the kidney or spleen are also involved in the clearance process but in a lesser degree. In non human primates treated with DMSA coated nanoparticles Perl's staining was positive in glomerulus capillaries as well as in the in the proximal convoluted tubules. This indicates the constant filtration and reabsortion of the iron[14]. In rats, iron is reabsorbed preferentially in the loops of Henle and collecting tubes. The use of AC susceptibility allowed us the distinction of the particles from other endogenous iron species, showing no nanoparticle accumulation in kidney tissues. In our study DMT1 concentration was increased in the kidneys, but this does not necessarily indicate the accumulation of nanoparticles in this organ, but probably a role recycling the products generated as a consequence from the particle degradation in other tissues.

Nanoscale

ARTICLE

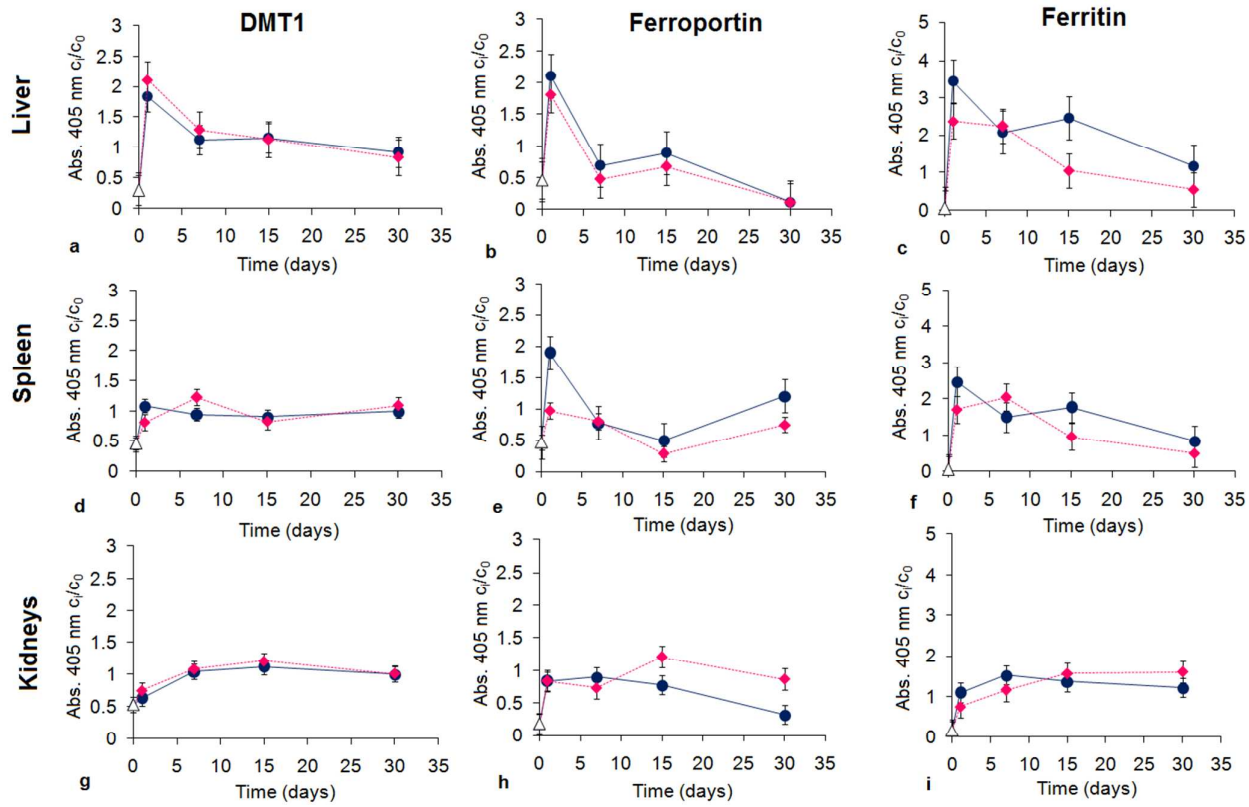

Figure 4. Variation of the concentration of different proteins involved in iron metabolic pathway determined by ELISA: DMT1, Ferroportin and Ferritin. (a-c) Liver, (d-f) Spleen and (g-i) Kidneys. (n=4/group per time point) Values indicated mean ± SD. [Control Δ, NP-DMSA ●, NP-PEG-$(NH_2)_2$ ♦]

After 7 days we observed that the concentration of these proteins decreased in the liver with a tendency to return to baseline values approximately at 30 days. This tendency to decrease could be explained because of the presence of iron regulatory proteins (IRP-1 and IRP-2). The activity of these proteins under excess conditions of iron, blocks the synthesis of DMT-1 in the cytoplasm of cells, ferroportin and transferrin receptor, while ferritin production is activated. Ferritin concentration remains elevated over basal levels for longer periods with the aim of storing iron excess in the body[37].

Conclusions

We have investigated here the effect of the coating on the evolution of magnetic nanoparticles in different organs after intravenous injection in a rat model. We have found not only species differences on nanoparticle biodistribution but also a dose-response relationship in the nanoparticle metabolism. The present findings show that both, DMSA and PEG coated particles undertake a quick transformation process under moderate doses in rats that in the case of DMSA is faster and leads to the quick appearance of ferritin. Both of them are good candidates for biomedical applications such as cancer research and clinical diagnosis since the possible toxicity associated to its accumulation after intravenous injection is null and its degradation follows

natural paths for biological metabolization of iron compounds.

The AC susceptibility data were corroborated by histological and iron metabolic proteins analysis, showing that this technique is an accurate method for the detection and quantification of magnetic nanoparticles in biological systems and also for the study of their degradation. This is a sensitive and selective method able to discriminate the magnetic signal of the injected particles from other iron endogenous species.

Acknowledgements

Amalia Ruiz holds a predoctoral fellowship from a CSIC-CITMA collaborative project (B01CU2009; ICMM, 2011-2014) and a short-term fellowship from CNPq (DTI-2; 383934/2013-3). Lucía Gutiérrez is the beneficiary of a post-doctoral grant from the AXA Research Fund. This work was partially supported by the European Commission (MULTIFUN, no. 262943).

References

1. S. Laurent and M. Mahmoudi, *International Journal of Molecular Epidemiology and Genetics*, 2011, **2**, 367-390.

2. M. Colombo, S. Carregal-Romero, M. F. Casula, L. Gutierrez, M. P. Morales, I. B. Bohm, J. T. Heverhagen, D. Prosperi and W. J. Parak, *Chemical Society reviews*, 2012, **41**, 4306-4334.

3. L. H. Reddy, J. L. Arias, J. Nicolas and P. Couvreur, *Chemical reviews*, 2012, **112**, 5818-5878.

4. A. Singh and S. K. Sahoo, *Drug Discovery Today*, 2013.

5. A. Ruiz, P. C. Morais, R. B. Azevedo, Z. G. M. Lacava, A. Villanueva and M. P. Morales, *Journal of Nanoparticle Research*, 2014, **16**.

6. S. Laurent, C. Burtea, C. Thirifays, U. O. Hafeli and M. Mahmoudi, *PloS one*, 2012, **7**, e9997.

7. R. Mejías, L. Gutiérrez, G. Salas, S. Pérez-Yagüe, T. M. Zotes, F. J. Lázaro, M. P. Morales and D. F. Barber, *Journal of Controlled Release*, 2013, **171**, 225-233.

8. A. Ruiz, Y. Hernández, C. Cabal, E. González, S. Veintemillas-Verdaguer, E. Martínez and M. P. Morales, *Nanoscale*, 2013, **5**, 11400-11408.

9. L. Yang, H. Kuang, W. Zhang, Z. P. Aguilar, Y. Xiong, W. Lai, H. Xu and H. Wei, *Nanoscale*, 2015, **7**, 625.

10. Y. Javed, L. Lartigue, P. Hugounenq, Q. L. Vuong, Y. Gossuin, R. Bazzi, C. Wilhelm, C. Ricolleau, F. Gazeau and D. Alloyeau, *Small*, 2014, **10**, 3325-3337.

11. C. Xu and S. Sun, *Advanced drug delivery reviews*, 2013, **65**, 732-743.

12. L. Gutiérrez, R. Mejías, D. F. Barber, S. Veintemillas-Verdaguer, C. J. Serna, F. J. Lázaro and M. P. Morales, *Journal of Physics D: Applied Physics*, 2011, **44**, 255002.

13. A. Ruiz, G. Salas, M. Calero, Y. Hernández, A. Villanueva, F. Herranz, S. Veintemillas-Verdaguer, E. Martínez, D. F. Barber and M. P. Morales, *Acta biomaterialia*, 2013, **9**, 6421-6430.

14. V. Monge-Fuentes, M. P. García, M. C. Tavares, C. R. Valois, E. C. Lima, D. S. Teixeira, P. C. Morais, C. Tomaz and R. B. Azevedo, *Nanomedicine : nanotechnology, biology, and medicine*, 2011, **6**, 1529-1544.

15. M. P. Garcia, R. M. Parca, S. B. Chaves, L. P. Silva, A. D. Santos, Z. G. M. Lacava, P. C. Morais and R. B. Azevedo, *Journal of Magnetism and Magnetic Materials* 2005, **293**, 277-282.

16. S. Kommareddy and M. Amiji, *Journal of pharmaceutical sciences*, 2007, **96**, 397-407.

17. A. Villanueva, M. Canete, A. G. Roca, M. Calero, S. Veintemillas-Verdaguer, C. J. Serna, M. P. Morales and R. Miranda, *Nanotechnology*, 2009, **20**, 115103.

18. L. Lartigue, D. Alloyeau, J. Kolosnjaj-Tabi, Y. Javed, P. Guardia, A. Riedinger, C. Péchoux, T. Pellegrino, C. Wilhelm and F. Gazeau, *ACS Nano*, 2013, **28**, 3939-3952.

19. M. Levy, F. Lagarde, V. A. Maraloiu, M. G. Blanchin, F. Gendron, C. Wilhelm and F. Gazeau, *Nanotechnology*, 2010, **21**, 395103.

20. D. Soukup, S. Moise, E. Céspedes, J. Dobson and N. D. Telling, *ACS Nano*, 2015, **9**, 231-240.

21. O. H. Lowry, N. J. Rosebrough, A. L. Farr and R. J. Randall, *The Journal of biological chemistry*, 1951, **193**, 265-275.

22. L. Gutiérrez, M. P. Morales and F. J. Lázaro, *Physical Chemistry Chemical Physics*, 2014, **16**, 4456-4464.

23. L. Gutierrez, F. J. Lazaro, A. R. Abadia, M. S. Romero, C. Quintana, M. P. Morales, C. Patino and R. Arranz, *Journal of inorganic biochemistry*, 2006, **100**, 1790-1799.

24. G. Salas, C. Casado, F. Teran, R. Miranda, C. J. Serna and M. P. Morales, *Journal of Materials Chemistry*, 2012, **22**, 21065.

25. Y. Ikeda and Y. Nagasaki, *Advances in Polymer Science*, 2011, **247**, 115-140.

26. R. E. Mebius and G. Kraal, *Nature Reviews Immunology*, 2005, **5**, 606-616.

27. P. Greaves, *Histopathology of preclinical toxicity studies. Interpretation and relevance in drug safety evaluation*, 2012.

28. L. Gutiérrez, R. Mejías, F. J. Lázaro, C. J. Serna, D. F. Barber and M. P. Morales, *IEEE Transactions on Magnetics*, 2013, **49**, 398-401.

29. S. B. Chaves, L. M. Lacava, Z. G. M. Lacava, O. Silva, F. Pelegrini, N. Buske, C. Gansau, P. C. Morais and R. B. Azevedo, *IEEE Transactions on magnetics*, 2002, **38**, 3231-3233.

30. R. Mejias, S. Perez-Yague, L. Gutierrez, L. I. Cabrera, R. Spada, P. Acedo, C. J. Serna, F. J. Lazaro, A. Villanueva, P. Morales Mdel and D. F. Barber, *Biomaterials*, 2011, **32**, 2938-2952.

31. L. Gutierrez, M. Vujic-Spasic, M. U. Muckenthaler and F. J. Lazaro, *Biochimica et Biophysica Acta (BBA) - Molecular Basis of Disease*, 2012, **1822**, 1147-1153.

32. R. R. Crichton, *Inorganic Biochemistry of Iron Metabolism From Molecular Mechanisms to Clinical Consequences*, John Wiley & Sons, Ltd, Baffins Lane, Chichester, England, 2001.

33. L. Gutierrez, K. Zubow, J. Nield, A. Gambis, B. Mollereau, F. J. Lazaro and F. Missirlis, *Metallomics : integrated biometal science*, 2013, **5**, 997-1005.

34. J. D. Lopez-Castro, J. J. Delgado, J. A. Perez-Omil, N. Galvez, R. Cuesta, R. K. Watt and J. M. Dominguez-Vera, *Dalton transactions*, 2012, **41**, 1320-1324.

35. S. Chamorro, L. Gutierrez, M. P. Vaquero, D. Verdoy, G. Salas, Y. Luengo, A. Brenes and F. J. Teran, *Nanotechnology*, 2015, **26**, 205101.

36. M. Levy, N. Luciani, D. Alloyeau, D. Elgrabli, V. Deveaux, C. Pechoux, S. Chat, G. Wang, N. Vats, F. Gendron, C. Factor, S. Lotersztajn, A. Luciani, C. Wilhelm and F. Gazeau, *Biomaterials*, 2011, **32**, 3988-3999.

37. N. C. Andrews, *The New England Journal of Medicine*, 1999, **341**, 1986-1995.